Modification of electro-optical properties of an orthoconic chiral biphenyl smectogen with its isostructural carborane analogue†

Wiktor Piecek,[b] Kristin L. Glab,[a] Adam Januszko,[a] Pawel Perkowski[b] and Piotr Kaszynski*[a]

Received 23rd July 2008, Accepted 21st November 2008
First published as an Advance Article on the web 22nd January 2009
DOI: 10.1039/b812633j

The effect of isostructural carborane additive **2F** on the phase structure, transition temperatures, and electrooptical properties of orthoconic biphenyl mesogen **1F** was investigated with thermal, electro-optical, dielectric, and XRD methods. Dielectric and optical data demonstrated that addition of 10 mol% of **2F** to **1F** maintains the orthoconic properties, while 20 mol% of **2F** changes the tilt angle to 40°. In both mixtures the helical pitch p_o is significantly shorter than in the host, which results in lower dielectric permittivity. Spontaneous polarization P_s remains practically unchanged upon addition of **2F**, while the viscosity is systematically lowered and, consequently, switching time is shortened by up to 25%. Comprehensive analysis of the three materials (the host and the two solutions) revealed that the carborane dopant affects primarily the interlayer intermolecular interactions, which manifests itself in tighter pitch and consequently in higher relaxation frequency f_r and elastic constant K_φ.

Introduction

Surface-stabilized ferroelectric (SSFLC) and antiferroelectric (SSAFLC) liquid crystals promise shorter switching times, a better gray scale, a broad viewing angle, inherent DC compensation, and driving voltages suitable for integrated drivers.[1,2] However, commercial applications of these materials have been hampered by imperfect optical uniformity of the relaxed state and light leakage in the tristable mode of SSAFLC caused by so-called pretransitional effects.[3] New possibilities in solving these problems appeared with the development of surface-stabilized orthoconic antiferroelectric liquid crystals (SSOAFLC), which typically contain a partially fluorinated alkyl substituent.[4–8] Molecules in this rare class of mesogens adopt 45° tilt angle θ in a single layer and 90° alternating tilt angle from one smectic layer to another.[9] Consequently, in the surface stabilized geometry and zero external electric field, the OAFLCs form a medium which is optically uniaxial and optically negative with the optical axis perpendicular to the OAFLC slab. From the application point of view, the most important property of SSOAFLC is the perfectly black texture between crossed polarizers regardless of the local defects. The optical contrast obtained upon driving the SSOAFLC is limited practically only by the quality of the polarizers.[3,9]

Technological applications of O(A)FLC require optimization of a number of properties including helical pitch, spontaneous polarization, rotational viscosity and elastic constants.[10] For instance, typical O(A)FLC materials exhibit short helical pitch, which makes it difficult to avoid pretransitional effects and light leakage.[5,10] It is also desired that such O(A)FLC and also (A)FLC materials in general exhibit nematic and smectic A phases to achieve proper alignment during device fabrication. Optimization of bulk properties is typically accomplished by structural modifications of (A)FLC compounds and the use of functionalized dopants.[5,11–13] Carborane-containing liquid crystals[14–33] could potentially help to address these challenges in FLC and AFLC device engineering and performance. Particularly relevant in this context are the nematogenic character[19,21,23–29,33] and low helical twisting power of chiral carborane mesogens.[26] It is also possible that additives containing the relatively bulky carborane will reduce the electrooptical switching time of (A)FLC materials as was observed for a sterically demanding dopant.[34]

To make the first step in the development of an effective carborane-containing additive for SS(A)FLC, we focused on a relatively simple and well-understood high-tilt ferroelectric biphenyl derivative **1F**,[4,11,35] and designed its carborane analogue **2F** in which the carborane cage is substituted for a benzene ring in the molecular rigid core (Fig. 1). We expected that such a design of **2F** would ensure its best compatibility with the biphenyl host and permit direct analysis of structural effects on mesogenic and electrooptical properties of the mesogen.

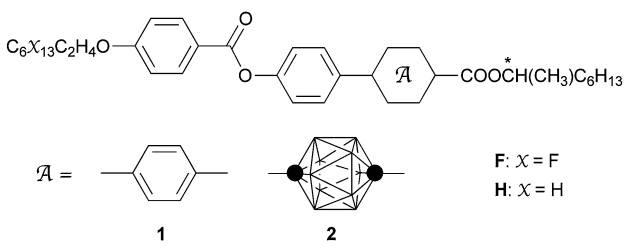

Fig. 1 Molecular structures of compounds **1** and **2**. In **2** each vertex represents a BH fragment and each sphere is a carbon atom.

[a]*Organic Materials Research Group, Department of Chemistry, Vanderbilt University, Nashville, TN, 37235, USA. E-mail: piotr.kaszynski@vanderbilt.ed; Fax: +1-615-343-1234; Tel: +1-615-322-3458*
[b]*Military University of Technology, Institute of Applied Physics, 00-908 Warsaw, Poland*

† Electronic supplementary information (ESI) available: Synthetic details, electrooptical data, computational results. See DOI: 10.1039/b812633j

Here, we report the preparation of carborane-containing chiral derivative **2F**, its mesogenic behavior, and investigation of its role as an additive in modifying the mesogenic and electro-optical properties of its benzene analog **1F**. We also assess the effect of tail fluorination on the mesophase structure and stability of **1F** and **2F** by comparison with the non-fluorinated analogs **1H**[36] and **2H** (Fig. 1). The pure compounds and their binary mixtures were investigated by thermal, optical, electro-optical, dielectric and XRD methods. The structural investigations were aided with *ab initio* molecular modeling of **1F** and **2F** molecules.

Results

Synthesis

Mesogens **1** and **2** were prepared by esterification of carboxylic acid **3** with phenols **4** and **5**, respectively, using dicyclohexylcarbodiimide (DCC) and catalytic amounts of 4-dimethylaminopyridine (DMAP), as shown in Scheme 1.

Phenol **5** was prepared in four steps from *p*-carborane as shown in Scheme 2. The copper derivative of *p*-carborane was arylated with 4-iodobenzyloxybenzene according to a general method[37] to yield the monoaryl derivative **6**. Lithiation of the second acidic carbon on the carborane moiety allowed efficient carboxylation. The resulting carboxylic acid **7** was esterified with (S)-2-octanol to form **8**. Finally, the benzyl protecting group was reductively removed to provide phenol **5** in 30% overall yield.

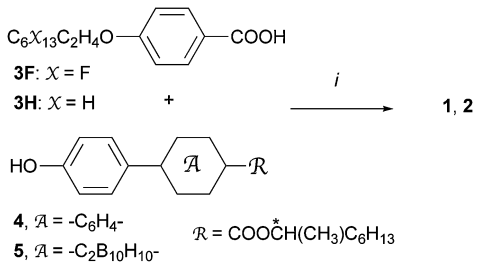

Scheme 1 *i*: DCC, DMAP, CH_2Cl_2.

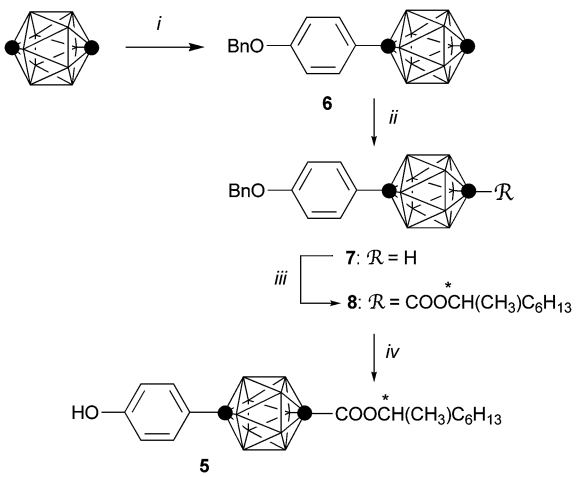

Scheme 2 *i*: 1. *n*-BuLi, 2. CuCl, 3. Et_3N, 4-BnO-C_6H_4-I, 65%. *ii*: 1. *n*-BuLi, 2. CO_2, 3. aq HCl, 90%. *iii*: (S)-2-octanol, DCC, DMAP, CH_2Cl_2, 53%. *iv*: H_2, Pd/C, 95%.

Preparations of phenol **4**[38] and carboxylic acid **3F**[39] are described elsewhere.

Thermal properties

Transition temperatures and associated enthalpies for compounds **1** and **2** are shown in Table 1. Phase structures were assigned by comparison with published textures for reference compounds and established trends in thermodynamic stability.[40–42]

Both benzene derivatives **1H** and **1F** exhibit enantiotropic smectic behavior. Partial fluorination of the octyloxy chain significantly increases the clearing transition temperature of **1H** and induces a ferroelectric SmC* phase (formerly SmC_β*)[43] in **1F**.[11] In contrast to the benzene analogs, the non-fluorinated carborane derivative **2H** exhibits only nematic behavior, which is typical for carborane-containing mesogens.[19,21,23–29,33] In addition, a platelet texture characteristic for the blue phase (BP) was observed upon slow heating of the monotropic chiral nematic phase of **2H**. Partial fluorination of the alkoxy chain of **2H** increased the mesophase stability and replaced the nematic phase with a monotropic SmA* phase in **2F**. The SmA* phase could be supercooled by about 20 K below melting but no SmC* was observed.

In agreement with other comparative studies, Table 1 shows that benzene derivatives **1** have greater mesophase stability than carborane derivatives **2**.[19,22,23,25,26]

Molecular modeling

Full geometry optimization of molecular structures of fluorinated smectogens **1F** and **2F** was performed at the HF/6-31G(d) level of theory.[44] The input structures were set in the most extended conformations and the optimized structures were perturbed several times until final geometries, shown in Fig. 2, were achieved. Results demonstrate that both molecules are hockey-stick-shaped with the hexyl group propagating from the chirality center at an angle of about 45° to the long axes of the rigid core. The projections of both molecules, **1F** and **2F**, on the *xz* plane parallel to the long axis of inertia (*x* axis in Fig. 2) are about 35.6 Å long. Analysis of both models shows that the–CH_2O– and–CO– fragments are coplanar with the adjacent benzene ring (Fig. 2), and the two benzene rings in the phenyl benzoate fragments form similar dihedral angles of 64° in **1F** and 61° in **2F**. These structural features are consistent with those found in solid-state structures of other mesogenic esters.[45] The perfluorohexyl group in both molecules adopts a helical conformation with the angle between the terminal C–C bonds (CF_3–$CF_2CF_2CF_2CF_2$–CF_2) of about 43°. This is consistent with the solid-state structures of other perfluoroalkyl groups,[46,47] and has been attributed to minimization of steric interactions of the fluorine atoms.[48] The dihedral angle in the biphenyl fragment of **1F** was optimized at 44°, which is consistent with the experimental gas phase structure for the parent biphenyl.[49] The Ph–carborane and also carborane–COO fragments form nearly eclipsed conformations, which permit the Ph and COO fragments to adopt a coplanar orientation. The C═O···C═O dihedral angle in the biphenyl derivative **1F** was optimized at 154°. In contrast, the five-fold rotational axes of the carborane cluster permit a better

Table 1 Transition temperatures (°C) and enthalpies (kJ mol^{-1}) for compounds **1** and **2**[a]

X	**1** $C_6X_{13}C_2H_4O$–Ph(=O)O–Ph–Ph–$COOCH(CH_3)C_6H_{13}$										**2** $C_6X_{13}C_2H_4O$–Ph(=O)O–Ph–carborane–$COOCH(CH_3)C_6H_{13}$					
F	Cr_1	94 (26.4)	Cr_2	98 (0.1)	SmC*	155 (1.2)	SmA*	185 (4.6)	I[b]		Cr	97 (34.0)	(SmA*	93) (1.4)	I	
H	Cr	93 (31.9)	SmA*	130 (5.8)	I[d]						Cr	36 (28.1)	(N*	21	BP	22)[c] I

[a] Cr = crystal, Sm = smectic, N = nematic, I = isotropic. In parentheses monotropic transitions. [b] Lit:[11] Cr_1 94.3 Cr_2 97.9 SmC_β* 155.6 SmA* 184.6 I. [c] Microscopic observation. [d] Lit:[36] Cr 92.5 SmA 130.8 I.

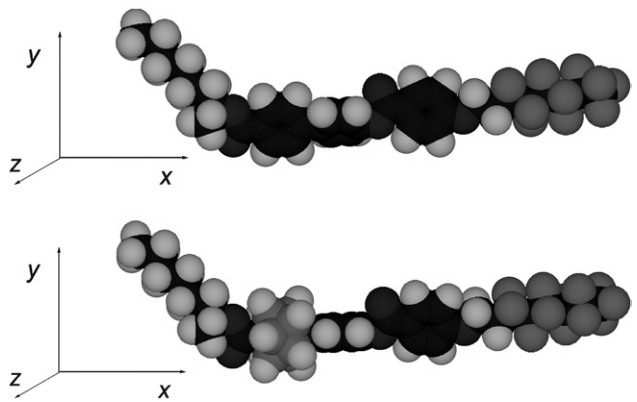

Fig. 2 Space-filling models for **1F** (top) and **2F** (bottom) obtained by full geometry optimization at the HF/6-31(d) level of theory. Models are shown in the Gaussian standard orientation.

adjustment of the relative orientation of the two carbonyl groups, which adopt a nearly antiparallel orientation in the optimized structure of **2F** (172°).

Ab initio calculations show that the carborane derivative **2F** has a smaller molecular dipole moment (0.61 D) than the biphenyl analog **1F** by 0.4 D.[50] The longitudinal component of the dipole moment in the former is practically 0 D, which results in the orthogonal orientation of the net dipole moment relative to the long molecular axis defined by the standard orientation. In contrast, the biphenyl analog **1F** has both dipole moment components significant ($\mu_{ll} = 0.58$ D and $\mu_{\perp} = 0.93$ D), which give rise to a 52° angle between the net dipole moment vector and the long molecular axis. The observed difference in the dipole moments of the two molecules arises from the conformational and electronic properties of the carborane moiety. The five-fold rotational symmetry of the carborane allows for nearly anti-planar alignment of the two carbonyl groups and significant lowering of the value of the transverse dipole moment component in **2F**. Also the electron withdrawing character of the carborane cage[27] combined with the electronegativity of the perfluorohexyl substituent completely compensate the local longitudinal dipole moment components of the two carboxyl groups.

Modification of bulk properties of 1F with 2F

The effect of the carborane additive **2F** on the physical properties of the orthoconic smectic host **1F** was investigated for two concentrations, mole fraction $x = 0.1$ and $x = 0.2$, and results for mixtures were compared to those for the pure host. The investigations included the additive's effect on the thermal, optical (tilt angle and helical pitch), electro-optical (spontaneous polarization and risetime), and dielectric properties of the host. The effect of **2F** on the layer spacing of the host was investigated by XRD methods.

DSC analysis revealed that addition of 10 mol% of **2F** to **1F** lowered all transition temperatures of the host by about 9 K (Fig. 3). The observed depression of the SmA*–I transition temperature is proportional to the concentration of the additive. In contrast, for solution $x = 0.2$ the SmA*–I transition temperature does not conform to the linear dependence on the concentration. The clearing temperature is depressed by 38 K, and the SmC* phase is destabilized by 34 K. The melting temperature for the $x = 0.2$ mixture is lower by about 34 K than those of either mixture's component.

Thermo-optical analysis of the binary mixtures in 1.6 μm cells with quasi-bookshelf alignment revealed similar non-linear changes of transition temperatures with concentration of carborane additive **2F** in biphenyl **1F**. The transition temperatures observed for material confined in the thin cell were however different from those measured in the free bulk phase. Thus, for $x = 0.1$ solution the SmA*–SmC* transition temperature of the host **1F** was lowered by 2 K, while for $x = 0.2$ solutions the SmC* phase was less stable by 11 K.[50] These temperatures obtained in the thin cell were used to define relative temperatures,[51] $\Delta T = T - T_{C\text{-}A}$, for comparison of the materials' parameters shown in Fig. 4–7, and 11–14.

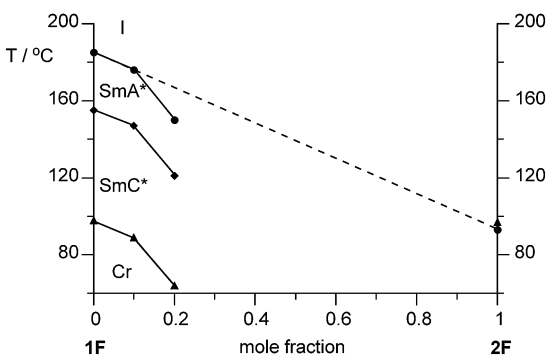

Fig. 3 Partial phase diagram for **2F** in **1F**. The dashed line connects SmA*–I phase transition points for the pure components.

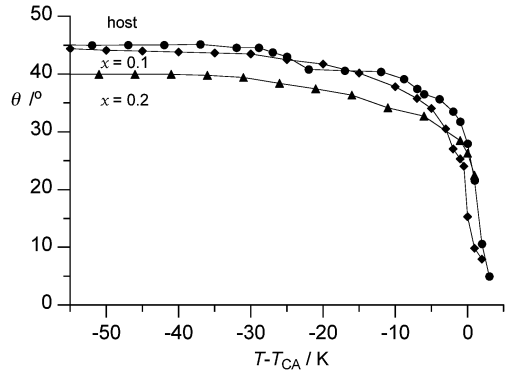

Fig. 4 The tilt angle θ as a function of relative temperature for pure host **1F** (circles) and 0.1 (diamonds) and 0.2 mole fraction (triangles) x of **2F** measured on cooling. Uncertainty $\pm 1^{\circ}$.

Investigation of the tilt angle θ confirmed[11,35] a nearly constant 45° tilt until 128 °C for the pure host **1F** (Fig. 4). At this temperature the observed value of θ is rapidly lowered by about 4°, and the new value θ of 41° remains nearly constant in the range of 135 °C–145 °C. At higher temperatures the tilt angle rapidly decreases until phase transition to SmA*. This pattern is fully reproducible in both the heating and the cooling modes. An addition of $x = 0.1$ mole fraction of **2F** does not significantly affect the tilt angle value of the host, while for the $x = 0.2$ solution the orthoconic property is lost and the saturated tilt angle θ is only 40°. The additive removes, however, the anomalous behavior of θ observed for the pure host at $\Delta T = -20$ K.

The wavelength of selective reflection λ for the host **1F** monotonously decreases with decreasing temperature from about 500 nm near the SmC*–SmA* phase transition to about 380 nm at $\Delta T = -40$ K (Fig. 5). An addition of $x = 0.1$ mole fraction of **2F** significantly tightens the helical pitch p, which is related to λ by the refractive index ($p = \lambda n^{-1}$), while 0.2 mole fraction of **2F** has surprisingly a much smaller effect on the pitch of the host. For instance, at a relative temperature of $\Delta T = -20$ K the wavelength of selective reflection λ for the $x = 0.1$ mixture is smaller by 53 nm than that of the pure host and for $x = 0.2$ mixture the difference is only 17 nm. Analysis of the curves shows much greater temperature dependence of λ for $x = 0.1$ mixture than for host or the $x = 0.2$ solution.

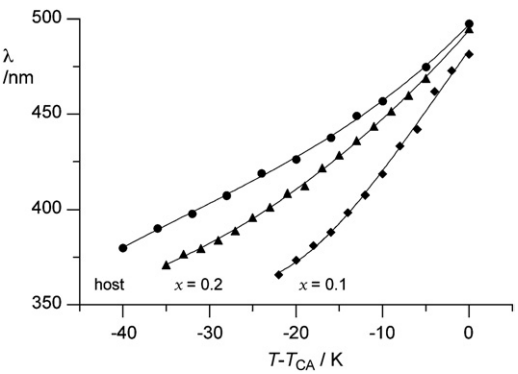

Fig. 5 The wavelength of selective reflection λ as a function of relative temperature for pure host **1F** (circles) and 0.1 (diamonds) and 0.2 mole fraction x (triangles) of **2F** obtained on cooling.

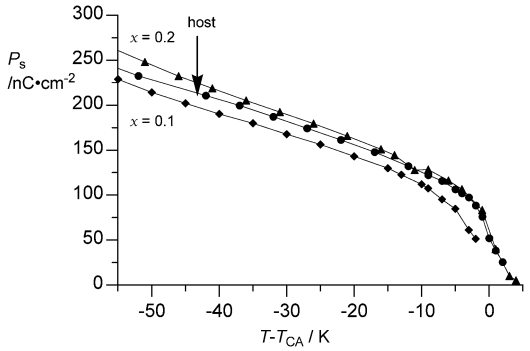

Fig. 6 Spontaneous polarization P_s as a function of relative temperature for pure host **1F** (circles) and 0.1 (diamonds) and 0.2 mole fraction x (triangles) of **2F** measured on cooling.

Spontaneous polarization of the host and the two mixtures is similar in the whole temperature range (Fig. 6). All three materials display nearly linear behavior of P_s(T) until about $\Delta T = -10$ K, at which temperature the P_s values begin a rapid decline. The $x = 0.1$ mixture of **2F** in **1F** have lower P_s values, while the P_s values for the $x = 0.2$ mixture appear to be slightly higher than those for the pure host. For instance, at $\Delta T = -25$ K, the P_s value for the $x = 0.1$ mixture is 8% smaller and for $x = 0.2$ is 3.5% larger than that for the pure host. The observed nearly linear behavior of the P_s(T) function away from the transition point is consistent with findings for orthoconic materials and rather rare for other types of ferroelectric smectics.[5]

The electro-optical risetime, τ_{10-90}, measured for the pure host **1F** is approximately a linear function of temperature and decreases from about 250 μs at $\Delta T = -50$ K to about 100 μs at $\Delta T = -10$ K (Fig. 7). Addition of either 0.1 or 0.2 mole fraction of **2F** reduces the host's risetime by about 25%. For instance, at $\Delta T = -25$ K both mixtures have shorter risetimes by about 40 μs than that of the pure host.

The measured risetime τ_{10-90} allowed the calculations of rotational viscosity γ_{φ} of the materials from equation 1 in which E is the electric field vector.[52] Results show that the viscosity of the biphenyl host, **1F**, is markedly lowered upon addition of carborane derivative **2F**, and that the higher the concentration of the additive the less viscous the material (Fig. 8). The Arrhenius

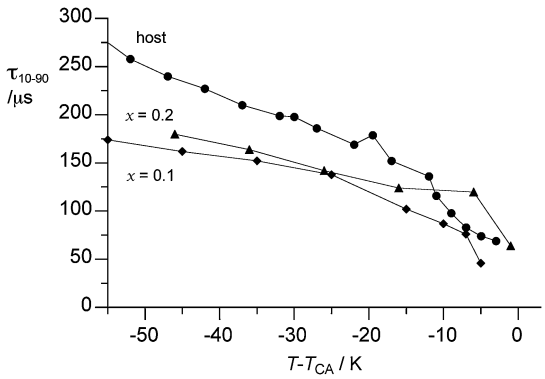

Fig. 7 The risetime τ_{10-90} as a function of relative temperature for pure **1F** (circles) and 0.1 (diamonds) and 0.2 mole fraction x (triangles) of **2F** measured on cooling.

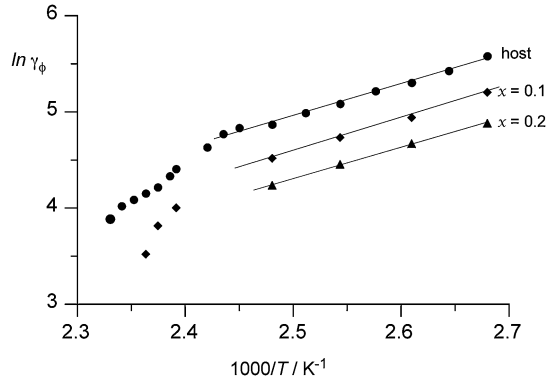

Fig. 8 The Arrhenius plot of rotational viscosity γ_ϕ for pure host **1F** (circles) and 0.1 (diamonds) and 0.2 mole fraction x (triangles) of **2F**.

analysis shows that within the experimental error the rotational viscosity activation energy E_a for the host and $x = 0.1$ mixture is practically the same and about 6.8 kcal/mol. In contrast, addition of 0.2 mole fraction of **2F** decreased the host's E_a to 6.4 ± 0.2 kcal/mol.

$$\gamma = \frac{1}{1.8}\tau_{10-90} \times P_s \times E \quad (1)$$

For a better understanding of molecular motions in the tilted phase, the host **1F** and its solutions with **2F** were analyzed using frequency domain dielectric spectroscopy (FDDS) in a broad temperature range. The materials were investigated in 20 μm cells to preserve the helical twist of the supramolecular structure of the SmC* phase, and were forced into a uniform quasi-bookshelf structure with smectic layers parallel to the direction of the applied electric field. For such an aligned material, the dielectric response was taken as the perpendicular component of the dielectric permittivity tensor $\varepsilon_\perp$, which was then decomposed to the real ($\varepsilon_\perp'$) and imaginary ($\varepsilon_\perp''$) parts according to the Cole–Cole relaxation model.[50,53]

Experimental results showed that the highest value of dielectric permittivity component $\varepsilon_\perp'$ (~120) was observed for the pure host **1F** in the SmC* phase (Fig. 9). An addition of 0.1 mole fraction of **2F** reduced the $\varepsilon_\perp'$ value to about 50, while the $x = 0.2$ solution had an intermediate value of about 80. This trend is consistent with the results of the pitch measurements (Fig. 5) and expected based on the theory[54] since $\varepsilon \sim p^2$. Analysis of the curves shows that the inclining character of the $\varepsilon_\perp'$(T) curve for the host in the tilted phase region was replaced with an almost temperature-independent characteristic measured for the two solutions with **2F**. Also the spike of the $\varepsilon_\perp'$ value due to the pretransitional effects (soft mode) increased with increasing concentration of the additive **2F**. These results are consistent with the theory[54,55] and general behavior of SmC* mixtures.[56–59]

The Cole–Cole analysis of the dielectric results recorded in a broad temperature range for the pure host **1F** and the two solutions with **2F** demonstrated only a single dielectric mode, the so-called Goldstone mode, present in the SmC* phase.[50] A plot of the imaginary part of the perpendicular component of the dielectric permittivity tensor $\varepsilon_\perp''$ in a 10 Hz–10 MHz frequency domain recorded at $\Delta T = -20$ K showed that the maximum of dielectric loss observed for the pure host **1F** at about 1 kHz was shifted to higher frequencies and its amplitude decreased upon addition of carborane derivative **2F** (Fig. 10). The dopant effect is non-monotonous and for the lower concentration ($x = 0.1$) the change is more pronounced than for higher concentration ($x = 0.2$) of **2F** in the host. This is consistent with the trends in the helical pitch values for the three materials (Fig. 5), since the frequency is proportional to p^{-2}.[60] Similar changes in the dielectric loss spectra were observed for other SmC* mixtures such as solutions of dichroic dyes in SmC* hosts.[56–59] The observed Wagner–Maxwell mode[55] in the low frequency region of the 20 mol% solution is due to ion conduction activated most likely by poor alignment uniformity and multi-domain structure of the sample.[55]

The dielectric data allowed for the calculation of the relaxation frequency f_r and dielectric strength $\Delta\varepsilon_G = \varepsilon_0 - \varepsilon_\infty$ from the Cole–Cole plots for each temperature, and results are shown in Fig. 11 and 12.[50] Subsequently, the results for dielectric strength $\Delta\varepsilon_G$ were used to calculate the twist elastic constant K_φ using equation 2,[54] and its temperature dependences for the host and the two solutions are shown in Fig. 13.

$$K_\varphi = \frac{p^2}{2\pi\varepsilon_0\Delta\varepsilon_G}\left(\frac{P_s}{\theta}\right)^2 \quad (2)$$

Results presented in Fig. 11–13 show again the non-monotonous dependence of phase parameters on the concentration of

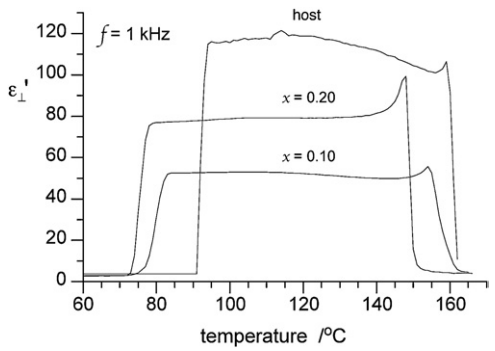

Fig. 9 The real part of the perpendicular component of the dielectric permittivity tensor $\varepsilon_\perp'$ as a function of temperature for pure **1F** (host) and its 0.1 and 0.2 mole fraction solutions with **2F** measured on cooling at 1 kHz.

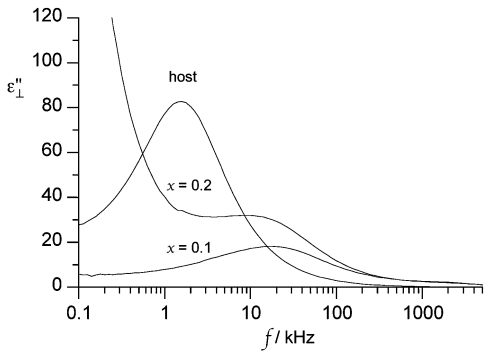

Fig. 10 The imaginary part of the perpendicular component of the dielectric permittivity tensor $\varepsilon_\perp''$ as a function of frequency for pure host **1F** (host) and its 0.1 and 0.2 mole fraction x solutions with **2F** measured at $\Delta T = -20$ K.

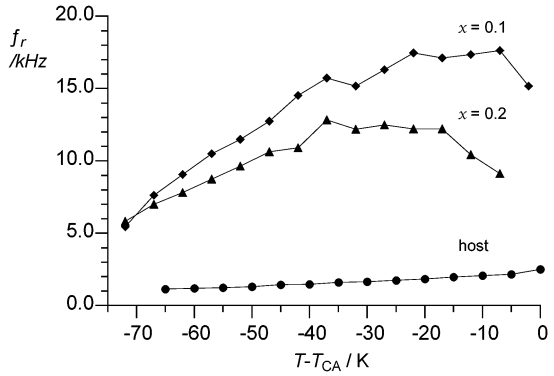

Fig. 11 The relaxation frequency f_r of the Goldstone mode vs. relative temperature $T - T_{AC}$ for pure host **1F** (circles), and 0.1 (diamonds) and 0.2 mole fraction x (triangles) of **2F**.

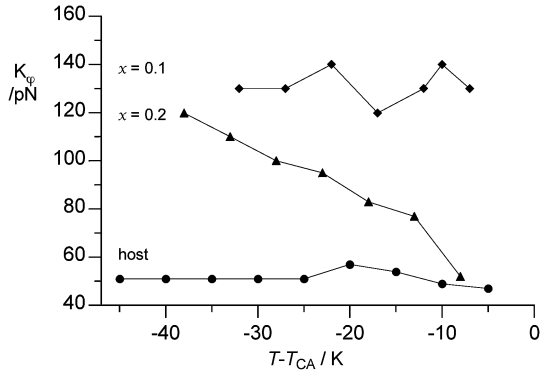

Fig. 13 Elastic constant K_φ vs. relative temperature $T - T_{AC}$ for pure host **1F** (circles), and 0.1 (diamonds) and 0.2 mole fraction x (triangles) of **2F**.

carborane derivative **2F** in the host; an addition of smaller amounts ($x = 0.1$) of **2F** gives larger change in the material's parameters than for the $x = 0.2$ solution. Analysis of the plot in Fig. 11 shows that the relaxation frequency f_r increases much faster with the temperature for the solutions than for the pure host. Also the character of the curves for the host and the two solutions is different. The former is steadily inclining, while those for the solutions have maximum at about $\Delta T = -25$ K. This behavior can be due to pretransitional effects and overlap of Goldstone and soft modes.

Fig. 12 shows that the dielectric strength $\Delta\varepsilon_G$ for the host declines rapidly, while for the solutions it is approximately constant away from the transition point. In the nearly linear region of the plot (ΔT range -70 K to -20 K) the gradient of the dielectric strength of the pure host is an order of magnitude greater (-1.24 ± 0.04 K^{-1}) that those for the 10 mol% (-0.11 ± 0.3 K^{-1}) and 20 mol% solutions (-0.10 ± 0.03 K^{-1}). The trends in Fig. 12 are consistent with results shown in Fig. 10.

The results in Fig. 13 demonstrate that the twist elastic constant K_φ for the pure host and for the 10 mol% solution weakly depends on the temperature, although the K_φ values for the latter are over 2 times greater than those for the pure host. In contrast, the twist elastic constant K_φ for $x = 0.2$ solution rapidly decreases with increasing temperature. This strong temperature dependence of K_φ for $x = 0.2$ is unexpected. Analysis of the parameters in equation 2 showed that for the $x = 0.2$ solution the ratio of $(P_s/\theta)^2$ has the steepest decline (-1.16, -0.93, and -1.6×10^{-7} C^2 m^{-4} K^{-1} for host, $x = 0.1$ and $x = 0.2$, respectively), while the $p^2/\Delta\varepsilon_G$ function has the weakest increasing character with increasing temperature (+13, +42, and $+8 \times 10^{-18}$ m^3 F^{-1} K^{-1} for host, $x = 0.1$ and $x = 0.2$, respectively). Thus, a combination of the two opposing trends, increasing for $p^2/\Delta\varepsilon_G$ and decreasing for $(P_s/\theta)^2$, gives a net decline of the K_φ (T) curve for the $x = 0.2$ solution, while for the host and $x = 0.1$ solution the two trends balance out and the K_φ (T) curves are practically temperature independent.

Small angle X-ray scattering measurements of the host **1F** in a broad temperature range revealed that the layer thickness in the SmA* phase is about 34 Å (Fig. 14). This value is about 1.5 Å smaller than the length of the molecular projection (Fig. 2), and the difference may be due to conformational flexibility of the terminal hexyl group. Addition of 0.1 mole fraction of **2F** slightly increased the layer spacing d. In contrast, the value d in $x = 0.2$ solution of **2F** was smaller by about 1 Å, which suggests either intercalation of the layers or more significant disorder of the hexyl chains. The formation of the de Vries phase[61] is unlikely, given the nearly temperature-independent d in the SmA* region and significant layer contraction by over 8% in the full SmA*–SmC* region.[62]

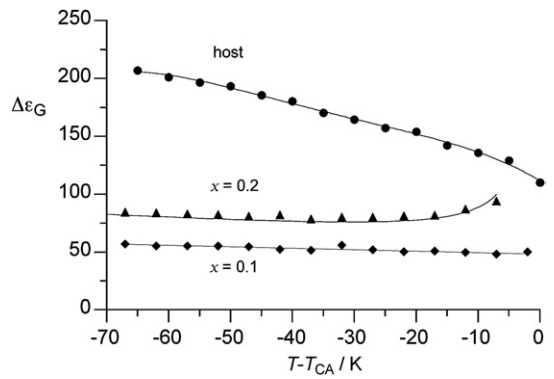

Fig. 12 The dielectric strength $\Delta\varepsilon_G$ vs. relative temperature $T - T_{AC}$ for pure host **1F** (circles), and 0.1 (diamonds) and 0.2 mole fraction x (triangles) of **2F**.

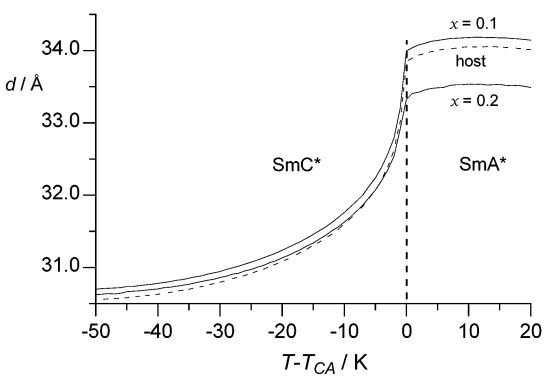

Fig. 14 The layer spacing d as a function of relative temperature for the pure host **1F** and 0.1 and 0.2 mole fraction x of **2F** measured on cooling by X-ray diffraction.

Upon cooling to the SmC* phase, the smectic layer spacing in all three materials monotonously decreases to about 30.7 Å in response to the molecule tilting. Considering the molecular length of 35.6 Å (Fig. 2), the tilt angle θ can be calculated at 30° to the layer normal. The resulting value θ is nearly 1.4 times smaller than that obtained from optical measurements (Fig. 4), which is consistent with the previous XRD analysis of **1F**[4] and typical for orthoconic materials.[5]

Discussion

Molecular modeling demonstrated that both fluorinated derivatives, biphenyl **1F** and carborane **2F**, have nearly identical static shapes and sizes in their most extended conformations (Fig. 2). However, their dynamic geometries are significantly different. Relative to benzene the carborane is larger (van der Waals diameter: 6.66 Å vs 7.43 Å),[63] moderately electron deficient,[64] and has a higher order of rotational axes. The benzene ring has a two-fold rotational symmetry axis along the C(1)···C(4) line, and the substituents may adopt one of two conformational minima (Fig. 15). In contrast, the carborane has C_5 symmetry axis and its derivatives have 5 conformational minima.[19,26] These geometrical and electronic differences between the two structural elements affect the number and distribution of conformational minima and also the magnitude and orientation of the dipole moment in their derivatives. Consequently, carborane derivatives, including **2F**, have generally higher conformational flexibility and smaller dynamic anisometry as compared to the benzene analogues such as **1F**. This manifests itself in typically lower clearing temperatures and far lower tendency to the formation of smectic phases,[19,23,24,27] even in mesogens with partially fluorinated alkyl chains[30,31] such as the pair of **1** and **2**. The larger size of the carborane and higher conformational mobility of its derivatives as compared to the carbocyclic analogues have been identified as plausible reasons for the observed markedly lower twisting power of a chiral carborane derivative.[26] In addition, such conformational mobility affects the magnitude of the transverse dipole moment, which in carborane derivatives can be minimized by fine adjustment of the relative orientation of local dipole moments, such as those of the carboxyl groups in **2F**. Therefore, it can be expected that these steric, conformational, and electronic properties of the carborane will result in low spontaneous polarization P_s and long supramolecular pitch p. The former is due to the relatively low stereo-polar coupling in carborane derivatives resulting from practically unhindered rotation of the C═O group in the vicinity of the chiral center,[65] and the latter to the shielding of the chiral center.

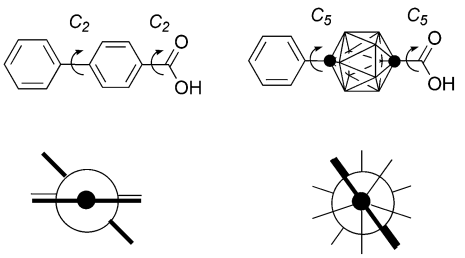

Fig. 15 Rotational axes and extended Newman projections for selected ground state conformers of model carboxylic acids. The bars represent the COOH (black) and the plane of the phenyl ring (gray).

Consequently, the addition of isostructural carborane derivative **2F** to the SmC* host **1F** should result in destabilization of the smectic phase, increase of the pitch p, and reduction of spontaneous polarization P_s. Experimental results demonstrated however that while the P_s indeed decreased in the 10 mol% solution relative to the pure host, the pitch significantly tightened and both parameters exhibit non-monotonous behavior in the binary system.

In general, carborane-containing mesogens and their carbocyclic analogues exhibit nearly linear dependence of clearing points (N–I transitions) on concentration in their binary mixtures.[14–16] Smectic phases are often destabilized in a non-linear mode by carborane additives, that do not exhibit smectic phases themselves.[14] Similar results were found for mixtures of carborane derivatives that are structurally related to **2F** and containing a partially fluorinated alkyl tail, with non-fluorinated carborane mesogens, and also their benzene analogues (compounds **9**).[30] Despite the fact that **2F** has a SmA* phase, experiments demonstrated that temperatures for both transition, SmA*–I and SmC*–SmA*, in the binary mixture of **1F** and **2F** exhibit non-linear character as a function of concentration.

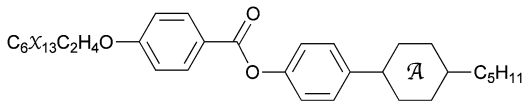

9 **a**: $\mathcal{X}$ = F **b**: $\mathcal{X}$ = H $\mathcal{A}$ = -C_6H_4-, -$C_2B_{10}H_{10}$-

Analysis of the optical and dielectric data demonstrated non-monotonous change of physical properties with increasing concentration of the dopant. Addition of 0.1 mole fraction of the carborane analog **2F** had little effect on the tilt angle θ, spontaneous polarization P_s, and the layer spacing d of the host **1F**. Therefore, it appears that **2F** is compatible with the biphenyl host at this concentration. However, measurements revealed a significantly tighter helix and, in consequence, significantly lower (by 60%) dielectric permittivity of the mixture as compared to those of the pure host **1F**. The mechanism of the observed pitch tightening is not clear at the moment, although occasionally observed in other systems.[66] Finally, the electro-optical measurements revealed that the rotational viscosity γ_φ of the mixture is markedly lower by about 25% than that of the pure host. This indicates that even 0.1 mole fraction of the additive is sufficient to increase the degree of freedom of molecules in the SmC* phase and presumably to enlarge free volume per molecule, which allows for less encumbered rotation in the electric field.

Addition of a larger amount of the carborane analog **2F** to the biphenyl host **1F** has a significant impact on all structural and physical parameters of the host. In general, parameters that were little affected by the 0.1 mole fraction of the additive **2F** were strongly changed in the $x = 0.2$ mixture. This includes layer spacing d and tilt angle θ. Effects of the additive on other parameters of the host such as the helical pitch p and dielectric permittivity were diminished, while the rotational viscosity γ_φ was reduced further in the temperature range of $\Delta T = > -25$ K as compared with the $x = 0.1$ mixture. Surprisingly, the value of spontaneous polarization P_s slightly exceeded that measured for the pure host.

Comprehensive analysis of the dielectric results for the host and the two solutions demonstrated that the K_φ is not the primary factor responsible for the low viscosity γ_φ. According to Eq 3 viscosity γ_φ depends on the elastic constant K_φ, pitch p, and relaxation frequency f_r.[55] Since the pitch p decreased upon doping the host, and the elastic constant increased, the decrease in the γ_φ is solely due to the high relaxation frequency f_r. This means that the helix is restored quickly upon distortion in an electric field.

$$\gamma_\varphi = \frac{2\pi K_\varphi}{f_r p^2} \quad (3)$$

Studies presented here for **1F** and **2F** constitute a rare example of detailed investigation of dopant effects on properties of a single component orthoconic ferroelectric SmC* phase.[66] There are only a handful of reported[11,67–69] studies of high tilt antiferroelectric compounds (OAFLC) in which the dopant was either structurally similar,[69] or a nematogen.[67] The latter studies demonstrated a nearly linear decrease of the P_s value, and a monotonous change of the tilt angle θ was implied for low concentrations ($x < 0.25$) of the nematic additive.[67] Unfortunately, the helical pitch could not be measured for low concentrations of the additive.[67] Other studies of binary mixtures of O(A)FLC were mostly limited to transition temperatures and helical pitch as a function of the composition.[11,68]

Studies of low-tilt ferroelectric materials are more numerous,[1] including ours.[22] Results show that the impact of the dopant on phase parameters varies depending on the host and the structure of the additive. In many such mixtures non-monotonous behavior of physical properties is often observed for low concentrations of the dopant.[66]

The limited body of data available for orthoconic mixtures demonstrates the complexity of the additive-host interactions and their effect on phase parameters. Better understanding of these effects and harnessing them for optimization of phase parameters will require more detailed and comprehensive studies using specifically design functional additives with systematically varied structural features.

Summary and conclusions

Comprehensive thermal optical and dielectric analysis showed that although carborane derivative **2F** does not exhibit a polar SmC* phase, it has a generally positive effect on some key parameters of the SmC* phase of its isostructural biphenyl host **1F**. Perhaps the most important effect of the carborane additive is the reduction of the switching time τ, while maintaining the high tilt angle θ and spontaneous polarization P_s of the host in low concentrations ($\leq$10 mol%). Contrary to expectations and desires, the carborane additive did not expand the host's helical pitch. Instead the pitch was tightened, which affected the dielectric and elastic parameters of the material. A full phase diagram for **1F** and **2F** and also for other close structural analogs would certainly be helpful for a better understanding of the impact of **2F** on phase parameters and the role played by the carborane additive **2F** on SmC* properties including the possibility of the formations of ferrielectric phases in this binary system.

Overall, results obtained for the pair **1F** and **2F** indicate that some carborane derivatives might be attractive dopants for fine-tuning of properties of orthoconic ferroelectric and possibly antiferroelectric materials. This warrants further studies of other carborane derivatives as functional modifiers of the SmC* materials and investigation of O(A)FLC materials containing their close structural carborane analogues.

Experimental

Optical microscopy and phase identification was performed using a PZO "Biolar" polarized microscope equipped with a HCS250 Instec hot stage. Thermal analysis was obtained using a TA Instruments 2920 DSC. Transition temperatures (onset) and enthalpies were obtained using small samples (2–3 mg) and a typical heating rate of 5 K min^{-1} under a flow of nitrogen gas. For DSC and microscopic analyses, each compound was additionally purified by dissolving in CH_2Cl_2, filtering to remove particles, condensing, and recrystallization from hexanes or a toluene/heptane mixture. The resulting crystals were dried under vacuum overnight at ambient temperature.

Binary mixtures were prepared by dissolving both components in small amounts of dry CH_2Cl_2, and subsequent evaporation of the solvent and drying the resulting homogeneous material at 70 °C for several hours. For mixtures the transition temperature was taken as the upper limit of the biphasic region as observed by optical microscopy.

Most of the structural and physical parameters were investigated by using previously published methods.[70] The tilt angle θ, spontaneous polarization P_s, switching time τ and rotational viscosity γ_ϕ were investigated using custom-built 1.6 μm thick cells coated with antiparallel rubbed polyimide (PI 2610, DuPont). The cells were filled with the material under study in the isotropic phase by capillary action. The uniform quasi-bookshelf structures with smectic layers parallel to the direction of the applied electric field were obtained during several slow cooling-heating cycles (~0.02 K min^{-1}) in the presence of an electric field (E $\approx$ 12 V μm^{-1}). Cells with the $x = 0.2$ mixture were subjected to twice as long an alignment process (more heating-cooling cycles) than the cells containing the host or the $x =$ 0.1 mixture. All measurements were performed on cooling from the isotropic phase at a rate of about 0.01 K min^{-1}. The same cells were used for thermo-optical analysis, and all electrooptical measurements.

The tilt angle θ was measured with the uncertainty of $\pm 1°$ using a standard method[71] as 1/2 of the rotation of the cell's optical axis of the fully extinguished states between crossed polarizers in an electric square wave field of 13.0 Vμm^{-1} and frequency of 20 Hz. The spontaneous polarization P_s ($\pm$2 nC cm^{-2}) was evaluated from the integration of the repolarization current peaks in the same cell as for the tilt angle measurements, under a triangle electric pulse at a frequency of 25 Hz.

For the evaluation of the switching time for the surface-stabilized FLC (SSFLC) structures of the orthoconic material, the smectic layer normal was oriented parallel with the incident light beam polarization. Upon the AC, square-shaped driving pulse, the optical axis of the structure switches between two bright states through the dark state. The switching time was evaluated as 90% of the time needed for the full switching between two bright states. The rotational viscosity was calculated from equation 1.[52]

Phase transition temperatures for the materials were determined in the same 1.6 μm thick cells on cooling by thermo-optical observations of the transmitted light intensity in a birefractive setup. The optical axis of the sample, defined in the SmC* phase, was oriented at the maximum transmission increment (22.5° off the orientation of the extinction maximum). Data and plots of the thermo-optical curves are shown in ESI.†

Dielectric measurements were performed in a broad temperature range in a frequency domain (total range 10 Hz–10 MHz; uncertainty of the frequency adjustment was <1% in the 500 Hz–1 MHz range) with a HP4192A impedance analyzer in 20 μm thick cells with gold electrodes covered with antiparallel rubbed polyimide (PI 2610, DuPont) to impose the quasi-bookshelf structure. The measuring AC voltage of 0.1 V was applied perpendicularly to the helical axis, which permitted observation of the perpendicular components (real $\varepsilon_\perp'$ and imaginary $\varepsilon_\perp''$) of the complex dielectric permittivity. The uncertainty of the evaluation of the $\varepsilon_\perp'$ and $\varepsilon_\perp''$ values is less than 0.5. Details of the Cole–Cole analysis are provided in ESI.†

The wavelength of selective reflection λ values (±2 nm) was measured for the samples placed on fresh, untreated glass and ordered by free surface upon slow cooling (0.02 K min^{-1}).

The smectic layer thickness as a function of temperature was obtained by small-angle X-ray scattering experiments at Warsaw University. All measurements were done on slow cooling of samples contained in a glass capillary placed in a temperature-controlled chamber using a Bruker diffractometer with a Cu lamp ($K_{\alpha 1}$) and a multilayers parabolic monochromator (Goebel mirror).

Acknowledgements

Financial support for this work was received from the National Science Foundation (DMR-0606317) and MUT (GD-980-2007). We are grateful to Prof. Roman Dabrowski for samples of **1F** and phenol **4**. The XRD analysis was kindly provided by Dr Damian Pociecha of Warsaw University, Poland. The helical pitch was measured by Ms Katarzyna Skrzypek of MUT, Warsaw, Poland. We thank Prof. Ewa Gorecka of Warsaw University, Poland, and Prof. Milada Glogarova from CAS, Prague, Czech Republic, for enlightening discussions.

References

1 S. T. Lagerwall,*Ferroelectric and Antiferroelectric Liquid Crystals*, New York, 1999, and references therein.
2 N. Yamamoto, N. Koshoubu, K. Mori, K. Nakamura and Y. Hamada, *Ferroelectrics*, 1993, **149**, 295–304.
3 (*a*) R. Beccherelli and S. J. Elston, *Liq. Cryst*, 1998, **25**, 573–577; (*b*) M. Johno, K. Itoh, J. Lee, Y. Ouchi, H. Takezoe, A. Fukuda and T. Kitazume, *Jpn. J. Appl. Phys*, 1990, **29**, L107–L110; (*c*) K. D'havé, P. Rudquist, S. T. Lagerwall, H. Pauwels, W. Drzewinski and R. Dabrowski, *Appl. Phys. Lett.*, 2000, **76**, 3528–3530.
4 R. Dabrowski, *Ferroelectrics*, 2000, **243**, 1–18.
5 R. Dabrowski, J. Gasowska, J. Otón, W. Piecek, J. Przedmojski and M. Tykarska, *Displays*, 2004, **23**, 9–19.
6 P. Morawiak, W. Piecek, M. Zurowska, P. Perkowski, Z. Raszewski, R. Dabrowski, K. Czuprynski and X. W. Sun, *Opto-electronics Rev.*, 2009, **17**, 40–44.
7 S. J. Cowling, A. W. Hall, J. W. Goodby, Y. Wang and H. F. Gleeson, *J. Mater. Chem.*, 2006, **16**, 2181–2191.
8 J. Gasowska, R. Dabrowski, W. Drzewinski, M. Filipowicz, J. Przedmojski and K. Kenig, *Ferroelectrics*, 2004, **309**, 83–93.
9 (*a*) K. D'havé, A. Dahlgren, P. Rudquist, J. P. F. Lagerwall, G. Andersson, M. Matuszczyk, S. T. Lagerwall, R. Dabrowski and W. Drzewinski, *Ferroelectrics*, 2000, **244**, 115–128; (*b*) S. T. Lagerwall, A. Dahlgren, P. Jägemalm, P. Rudquist, K. D'havé, H. Pauwels, R. Dabrowski and W. Drzewinski, *Adv. Funct. Mater.*, 2001, **11**, 87–94.
10 S. T. Lagerwall, *Ferroelectrics*, 2004, **301**, 15–45.
11 R. Dabrowski, J. M. Otón, V. Urruchi, J. L. Gayo, K. Czuprynski and S. Gauza, *Pol. J. Chem.*, 2002, **76**, 331–344.
12 M. J. O'Callaghan, M. Wand, C. Walker, W. Thurmes and K. More, *Ferroelectrics*, 2006, **343**, 201–207.
13 See also: V. Novotná, M. Glogarová, V. Hamplová and M. Kaspar, *J. Chem. Phys.*, 2001, **115**, 9036–9041; N. Éber, *Liq. Cryst.*, 2002, **29**, 1347–1354; V. Novotná, V. Hamplová, M. Kaspar, M. Glogarová, A. Bubnov and Y. Lhotáková, *Ferroelectrics*, 2004, **309**, 103–109; A. Bubnov, V. Novotná, V. Hamplová, M. Kaspar and M. Glogarová, *J. Mol. Struct.*, 2008, **892**, 151–157.
14 A. G. Douglass, K. Czuprynski, M. Mierzwa and P. Kaszynski, *J. Mater. Chem.*, 1998, **8**, 2391–2398.
15 A. G. Douglass, K. Czuprynski, M. Mierzwa and P. Kaszynski, *Chem. Mater.*, 1998, **10**, 2399–2402.
16 K. Czuprynski, A. G. Douglass, P. Kaszynski and W. Drzewinski, *Liq. Cryst.*, 1999, **26**, 261–269.
17 K. Czuprynski and P. Kaszynski, *Liq. Cryst.*, 1999, **26**, 775–778.
18 A. G. Douglass, B. Both and P. Kaszynski, *J. Mater. Chem.*, 1999, **9**, 683–686.
19 P. Kaszynski and A. G. Douglass, *J. Organomet. Chem.*, 1999, **581**, 28–38.
20 P. Kaszynski, S. Pakhomov, K. F. Tesh and V. G. Young, Jr., *Inorg. Chem.*, 2001, **40**, 6622–6631.
21 W. Piecek, J. M. Kaufman and P. Kaszynski, *Liq. Cryst.*, 2003, **30**, 39–48.
22 A. Januszko, P. Kaszynski, M. D. Wand, K. M. More, S. Pakhomov and M. O'Neill, *J. Mater. Chem.*, 2004, **14**, 1544–1553.
23 K. Ohta, A. Januszko, P. Kaszynski, T. Nagamine, G. Sasnouski and Y. Endo, *Liq. Cryst.*, 2004, **31**, 671–682.
24 T. Nagamine, A. Januszko, K. Ohta, P. Kaszynski and Y. Endo, *Liq. Cryst.*, 2005, **32**, 985–995.
25 B. Ringstrand, J. Vroman, D. Jensen, A. Januszko, P. Kaszynski, J. Dziaduszek and W. Drzewinski, *Liq. Cryst.*, 2005, **32**, 1061–1070.
26 A. Januszko, P. Kaszynski and W. Drzewinski, *J. Mater. Chem.*, 2006, **16**, 452–461.
27 A. Januszko, K. L. Glab, P. Kaszynski, K. Patel, R. A. Lewis, G. H. Mehl and M. D. Wand, *J. Mater. Chem.*, 2006, **16**, 3183–3192.
28 T. Nagamine, A. Januszko, P. Kaszynski, K. Ohta and Y. Endo, *J. Mater. Chem.*, 2006, **16**, 3836–3843.
29 P. Kaszynski, A. Januszko, K. Ohta, T. Nagamine, P. Potaczek, V. G. Young, Jr. and Y. Endo, *Liq. Cryst.*, 2008, **35**, 1169–1190.
30 A. Januszko, K. L. Glab and P. Kaszynski, *Liq. Cryst.*, 2008, **35**, 549–553.
31 A. Januszko and P. Kaszynski, *Liq. Cryst.*, 2008, **35**, 705–710.
32 M. Jasinski, A. Jankowiak, A. Januszko, M. Bremer, D. Pauluth and P. Kaszynski, *Liq. Cryst.*, 2008, **35**, 343–350.
33 T. Nagamine, A. Januszko, K. Ohta, P. Kaszynski and Y. Endo, *Liq. Cryst.*, 2008, **35**, 865–884.
34 A. Yasuda and E. Matsul, *Eur. Pat.* EP 0808887, 1997.
35 J. Rutkowska, P. Perkowski, J. Kedzierski, Z. Raszewski, R. S. Dabrowski, S. Gauza, K. L. Czuprynski and E. Miszczyk, *Proc. SPIE-Int. Soc. Opt. Eng.*, 2000, **4147**, 101–108.
36 D. R. Medeiros, M. A. Hale, J. K. Leitko and C. G. Willson, *Chem. Mater.*, 1998, **10**, 1805–1813.
37 R. Coult, M. A. Fox, W. R. Gill, P. L. Herbertson, J. A. H. McBride and K. Wade, *J. Organomet. Chem.*, 1993, **462**, 19–29.
38 W. Drzewinski, K. Czuprynski, R. Dabrowski and M. Neubert, *Mol. Cryst. Liq. Cryst.*, 1999, **328**, 401–410.
39 L. Andruzzi, E. Chiellini, G. Galli, X. Li, S. H. Kang and C. K. Ober, *J. Mater. Chem.*, 2002, **12**, 1684–1692.
40 G. W. Gray, J. W. G. Goodby, *Smectic Liquid Crystals-Textures and Structures*; Leonard Hill: Philadelphia, 1984.
41 D. Demus, L. Richter, *Textures of Liquid Crystals*; 2nd ed.; VEB: Leipzig, 1980.
42 I. Dierking, *Textures of Liquid Crystals*; Wiley-VCH: Weinheim, 2003.

43 H. Takezoe, E. Gorecka and M. Copic, to appear in Rev. Modern Phys.
44 *Gaussian 98, Revision A.9*, M. J. Frisch, G. W. Trucks, H. B. Schlegel, G. E. Scuseria, M. A. Robb, J. R. Cheeseman, V. G. Zakrzewski, J. A. Montgomery, Jr., R. E. Stratmann, J. C. Burant, S. Dapprich, J. M. Millam, A. D. Daniels, K. N. Kudin, M. C. Strain, O. Farkas, J. Tomasi, V. Barone, M. Cossi, R. Cammi, B. Mennucci, C. Pomelli, C. Adamo, S. Clifford, J. Ochterski, G. A. Petersson, P. Y. Ayala, Q. Cui, K. Morokuma, D. K. Malick, A. D. Rabuck, K. Raghavachari, J. B. Foresman, J. Cioslowski, J. V. Ortiz, A. G. Baboul, B. B. Stefanov, G. Liu, A. Liashenko, P. Piskorz, I. Komaromi, R. Gomperts, R. L. Martin, D. J. Fox, T. Keith, M. A. Al-Laham, C. Y. Peng, A. Nanayakkara, M. Challacombe, P. M. W. Gill, B. Johnson, W. Chen, M. W. Wong, J. L. Andres, C. Gonzalez, M. Head-Gordon, E. S. Replogle, and J. A. Pople, Gaussian, Inc., Pittsburgh PA, 1998.
45 W. Haase, M. A. Athanassopoulou in *Structure and Bonding*; Mingos, D. M. P., Ed.; Springer: Berlin, 1999; Vol. 94, p 139–197.
46 P. Kromm, J.-P. Bideau, M. Cotrait, C. Destrade and H. Nguyen, *Acta Cryst. C*, 1994, **50**, 112–115.
47 M. Yano, T. Taketsugu, K. Hori, H. Okamoto and S. Takenaka, *Chem. Eur. J.*, 2004, **10**, 3991–3999.
48 C. W. Bunn and E. R. Howells, *Nature*, 1954, **174**, 549–551.
49 A. Almenningen, O. Bastiansen, L. Fernholt, B. N. Cyvin, S. J. Cyvin and S. Samdal, *J. Mol. Struct.*, 1985, **128**, 59–76.
50 For details see ESI†.
51 Relative temperature is defined as a difference between actual and reference temperatures, while reduced temperature is typically expressed as a ratio of the two temperatures.
52 K. Skarp, *Ferroelectrics*, 1988, **84**, 119–142.
53 K. S. Cole and R. H. Cole, *J. Chem. Phys*, 1941, **9**, 341–351; K. S. Cole and R. H. Cole, *J. Chem. Phys*, 1942, **10**, 98–105.
54 T. Carlsson, B. Zeks, C. Filipic and A. Levstik, *Phys. Rev. A*, 1990, **42**, 877–889.
55 *Relaxation Phenomena*; W. Haase, S. Wróbel, Eds.; Springer Verlag, 2003, and references therein.
56 A. K. Srivastava, R. Manohar and J. P. Shukla, *J. Phys. Chem. Solids*, 2007, **68**, 1700–1706.
57 S. Khosla and K. K. Raina, *J. Phys. Chem. Solids*, 2004, **65**, 1165–1175.
58 K. K. Raina, A. K. Gathania and B. Singh, *J. Phys. Condens. Matter*, 1999, **11**, 7061–7069.
59 A. K. Srivastava, R. Manohar, J. P. Shukla and A. M. Biradar, *Jpn. J. Appl. Phys.*, 2007, **46**, 1100–1105.
60 J. Hmine, C. Legrand, N. Isaert and H. T. Nguyen, *J. Phys. Condens. Matter*, 2003, **15**, 4671–4677.
61 (*a*) J. P. F. Lagerwall, F. Giesselmann and M. D. Radcliffe, *Phys. Rev. E.*, 2002, **66**, 031703; (*b*) A. de Vries, *Mol. Cryst. Liq. Cryst.*, 1977, **41**, 27–31; (*c*) A. de Vries, A. Ekachai and N. Spielberg, *Mol. Cryst. Liq. Cryst.*, 1979, **49**, 143–152.
62 M. Krueger and F. Giesselmann, *Phys. Rev. E*, 2005, **71**, 041704.
63 Reference 33 in ref. 27.
64 The σ_p value for p-carborane is 0.14 (L. I. Zakharkin, V. N. Kalinin and E. G. Rys Bull, *Acad. Sci. USSR, Div. Chem. Sci.*, 1974, 2543–2545) while that for Ph is −0.01 (D. H. McDaniel and H. C. Brown, *J. Org. Chem.*, 1958, **23**, 420–427).
65 (*a*) D. A. Dunmur, M. Grayson and S. K. Roy, *Liq. Cryst.*, 1994, **16**, 95–104; (*b*) Z. Raszewski, J. Rutkowska, J. Kedzierski, P. Perkowski, W. Piecek, J. Zielinski, J. Zmija and R. Dabrowski, *Mol. Cryst. Liq. Cryst.*, 1995, **263**, 271–283, and 1997, 302, 85–91; (*c*) B. Urbanc, B. Zeks and T. Carlsson, *Ferroelectrics*, 1991, **113**, 219–230.
66 R. Dabrowski, personal communication.
67 J. P. F. Lagerwall, F. Giesselmann, C. Selbmann, S. Rauch and G. Heppke, *J. Chem. Phys.*, 2005, **122**, 144906.
68 For example: M. Tykarska, Z. Stolarz and J. Dziaduszek, *Ferroelectrics*, 2004, **311**, 51–57; E. Scibior, A. Samsel, K. Skrzypek and M. Tykarska, *Ferroelectrics*, 2006, **343**, 161–166.
69 For example: S. Gauza, K. Czuprynski, R. Dabrowski, K. Kenig, W. Kuczynski and F. Goc, *Mol. Cryst. Liq. Cryst.*, 2000, **351**, 287–296; R. Dabrowski, W. Drzewinski, K. Czuprynski, S. Gauza, K. Kenig, W. Kuczynski and F. Goc, *Mol. Cryst. Liq. Cryst.*, 2001, **365**, 199–211.
70 W. Piecek, Z. Raszewski, P. Perkowski, J. Kedzierski, J. Rutkowska, J. Zielinski, E. Nowinowski-Kruszelnicki, R. Dabrowski, M. Tykarska and J. Przedmojski, *Mol. Cryst. Liq. Cryst.*, 2005, **436**, 149–165.
71 S. Bezner, M. Krueger, V. Hamplová, M. Glogarová and F. Giesselmann, *J. Chem. Phys.*, 2007, **126**, 054902.

